



Research paper

Strength analysis of eccentrically loaded thin-walled steel lipped C-profile columns

Leszek Czechowski¹, Maria Kotelko², Jacek Jankowski³,
Viorel Ungureanu⁴, Annabella Sanduly⁵

Abstract: The work includes the results of numerical, analytical-numerical and experimental study into the influence of load eccentricities with regard to major axis on post-buckling behaviour and load-carrying capacity of thin-walled cold-formed steel lipped channel section columns. The study was solved by using the finite element method (code Ansys) with taking into consideration a full material characteristics in logarithmic strain system and geometric nonlinearities. The analytical-numerical solution was based on Koiter's theory with an application of finite difference method (FDM). Some chosen results of numerical simulations have been compared to experimental results. The deformations of columns were registered by means of Digital Image Correlation Aramis System (DICAS) to observe the maps and the magnitude of displacements for adequate point of a load. The analyses showed that the decrease in maximum load in a dependency on the eccentricity value can be even 3 times minor in a comparison to the load-carrying capacity of axially loaded column.

Keywords: thin-walled structures, load-carrying capacity, eccentric load, C-profile, Koiter's theory

¹PhD., Eng., Lodz University of Technology, Faculty of Mechanical Engineering, Stefanowskiego 1/15 street, 90-537 Lodz, Poland, e-mail: leszek.czechowski@p.lodz.pl, ORCID: 0000-0002-4718-6215

²Professor, DSc, PhD., Eng., Lodz University of Technology, Faculty of Mechanical Engineering, Stefanowskiego 1/15 street, 90-537 Lodz, Poland, e-mail: maria.kotelko@p.lodz.pl, ORCID: 0000-0001-7784-4349

³PhD., Eng., Lodz University of Technology, Faculty of Mechanical Engineering, Stefanowskiego 1/15 street, 90-537 Lodz, Poland, e-mail: jacek.jankowski@p.lodz.pl, ORCID: 0000-0002-9628-2799

⁴Professor, DSc, PhD., Eng., Department of Steel Structures and Structural Mechanics, Politehnica University of Timisoara, Romania, e-mail: viorel.ungureanu@upt.ro, ORCID: 0000-0002-5826-9518

⁵PhD Student, Lodz University of Technology, Faculty of Mechanical Engineering, Stefanowskiego 1/15 street, 90-537 Lodz, Poland, e-mail: annabella.sanduly@dokt.p.lodz.pl, ORCID: 0000-0003-0568-3181

1. Introduction

Thin-walled cold-formed steel (TWCFS) sections are widely used in various applications. Cold-formed steel profiles can be used for entire buildings and for complete roof, floor and wall systems (Fig. 1a) as well as racking systems (Fig. 1b) From structural point of view, the thin-walled cold-formed steel members can serve as both primary and secondary structures.

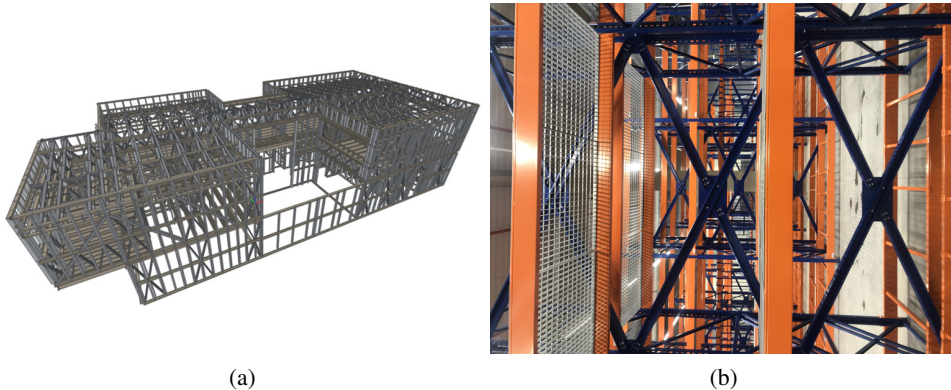


Fig. 1

Such steel components can have usually stiffening lips on flanges and/or intermediate stiffeners in wide flanges and webs. Both simple and complex shapes of profiles can be manufactured for structural and non-structural applications. The problem of buckling loads and the load-carrying capacity of TWCFS structures subjected to simple loading systems (pure bending, uniform compression, e.g.) has been solved with a good accuracy based on the theory of thin-walled structures as well as in design code specifications as EN 1993-1-3 [6], giving accurate predictions for the buckling load and ultimate strength of TWCFS structures especially under concentric axial compression. Looking at accessible literature, one can find a few reported results of both theoretical and experimental study on the structural behaviour of TWCFS columns under eccentric compression particularly with respect to major axis bending. In 1977 Rhodes and Harvey published the very first results of the research concerning the members of the channel section under eccentric compression [19]. Miller et al. [17] investigated the effect of load eccentricity in TWCFS long lipped channel sections with perforated and non-perforated webs. Mulligan et al. [18] proposed relations of the effective width of members of the lipped channel section under eccentric load with respect to the minor axis. They compared the ultimate load predictions obtained on this basis with the experimental results and code recommendations. Zhao et al. in papers [21, 22] analysed the columns with box-type and L-type sections made of aluminium alloy subjected to eccentric and stainless steel circular hollow sections under combined loads. Meng and Gardner in [16] investigated the

influence of yield strength on the in-plane stability and design of structural steel square and rectangular hollow section beam-columns under compression and uniform bending. Liang et al. [13, 14] studied the local cross-sectional behaviour of stainless steel channel sections subjected to the combined axial compression and minor axis bending moment. They conducted both the experiment and FE simulations. Based on a parametric study they performed a lot of analyses for a wider range of cross-section aspect ratios and slenderness, loading combinations and bending orientations. In other paper [15] of Liang et al., experimental and numerical results on the behaviour of laser-welded stainless steel channel sections under combined loads (compression and bending moment) about the major axis were presented. Zhang et al. in [23] investigated the buckling behaviour of press-braked stainless steel channel section beam-columns under combined compression and minor-axis bending. The performed FE simulations were based on different cross-section dimensions, member effective lengths and loading combinations. Both experimental and numerical results were referred to standard design rules. Their results partially covered with standards predictions. A continuation was a study by Zhang et al. in work [24], who analysed theoretically and experimentally press-braked stainless steel channel sections under combined compression and major axis bending moment. Based on FEM, Huang and Zhang in [7] investigated a high strength steel welded I-section overall buckling performance with respect to the major axis under combined loads (axial compression and bending). Li and Young in [12] showed the results of experimental tests executed on cold-formed steel built-up open section members (two back-to-back channel sections with intermediate stiffeners) under eccentric compressive load (compression and bending with respect to the minor axis). The tests were carried out for a wide range of column lengths and the eccentricities. They compared their results with the predictions of the North American Specification, European Code, Australian/New Zealand and American Standard. The comparisons showed in general that the interactive formulae for the axial load-moment underestimate the load-carrying capacities of the built-up open section of the cold-formed steel structures. Kotełko et al. in [11] presented the results of local plastic failure mechanisms for columns of the lipped channel section subjected to eccentric compression with respect to the minor axis. The continuance of aforementioned paper was work elaborated by Borkowski et al. [2] relating an experimental program into the post-failure behaviour of TWCFS members subjected to eccentric compression about the minor axis. They tested samples under compression load with a wide range of positive and negative eccentricities. Buchanan et al. in [3] studied experimentally and numerically the strength of stainless steel circular hollow section beam-columns subject to eccentric load. More than 2000 numerical results were done to determine new design proposals for stainless steel beam-columns. They proposed new approach which could be more realistic in predictions of load-carrying capacity in reference to the current EN 1993-1-4 code. Another authors in [4] analysed the behaviour of close-section cold-formed steel elliptical hollow members under eccentric compression. They validated FE models in relations to test results. They accomplished a wide parametric study and compared their results with the predictions of the design methods.

The present paper is continuance of recently performed investigations based on an assessment of the behaviour of steel lipped channel profiles subjected to eccentric load about major axis.

2. Subject of objective of research

Since the failure of short TWCFS members in compression or bending is always characterised by a local plastic mechanism, the possibility occurs to use the yield line analysis (YLA) to characterize the ultimate strength (to estimate upper bound load capacity) by combining post-buckling path with post-ultimate curve [9]. It is an alternative way to the effective width approach. Thus, the objective of the present research was to develop equilibrium path, determining the members structural behaviour in the whole range of loading, up to and beyond an ultimate load. The previous studies, mentioned above [2,9,20] were focused on the identification of plastic mechanisms of failure in the columns subjected to eccentric compression both about minor and major axis. The focus of this study is the numerical and experimental analysis of the structural behaviour of the members under eccentric compression about major axis, particularly on observations of deformation modes and theoretical derivation of pre- and post-buckling path, and, subsequently, validation of the theoretical (numerical) solutions via experiment. Pre- and post-buckling paths were derived not by using FE simulations, but FDM calculations as well. The latter is much less time consuming and gives an opportunity to develop relatively simple and general algorithms. Theoretical post-buckling path together with the post-ultimate curve obtained from YLA analysis [9], obtained also on the basis of simple algorithms, allows one to estimate an upper-bound load-carrying capacity.

The subject of investigation was the C-column subjected to eccentric load with regard to major axis (Fig. 2). The dimensions of columns are following: $l = 450$ mm, $a = 150$ mm, $b = 60$ mm, $c = 25$ mm. The eccentricity $e_x (\pm)$ ranged from 0 to 120 mm.

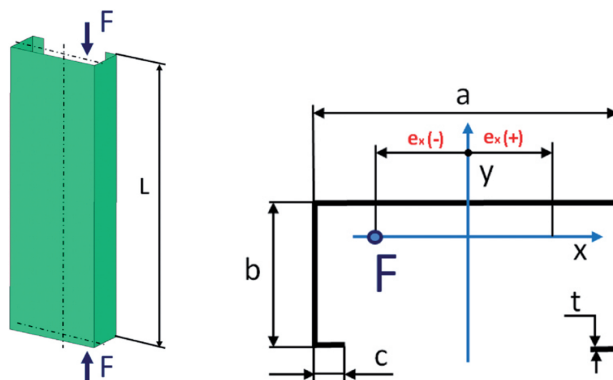


Fig. 2

3. Numerical models

Numerical models were based on two different methods. The first one was created based on finite element method (FEM). The second one was relied on finite difference method (FDM).

3.1. FE Model

Based on discrete model, computations were performed by using Ansys 18.2 software [1]. The mesh of numerical model was created by applying the 4-node 181-shell element suitable for moderate thin-walled structures. Based on calculation of the time consumption and accuracy, the size of the finite element was 2 mm. Based on Block Lanczos algorithm, buckling loads were determined. The nonlinear simulations were performed for large strains and the deflections on the basis of Green-Lagrangian equations. To achieve the computational convergence for large deformations of structures, the number of substeps was set from 2000 up to 50,000. In each substep, maximum number of iterations could come to 5000. FE model and the boundary conditions are showed in Fig. 3. The adequate eccentricity of the load applied to member took place thanks to two master nodes (upper and lower) linked to slave nodes being on outer edges of C-profiles. Nonlinear estimations and convergence analysis were conducted by using the Newton-Raphson algorithm. The perfect structures were taken into account to prevent from imposing some post-critical equilibrium path. The mean one-directional tensile curve (as the function of true stress vs. logarithmic strain) of material based on empirical tests as the true stress-logarithmic strain was elaborated (Fig. 4a – general view and Fig. 4b – limited range of stress and strain). Subsequently, the multi-linear material model was applied.

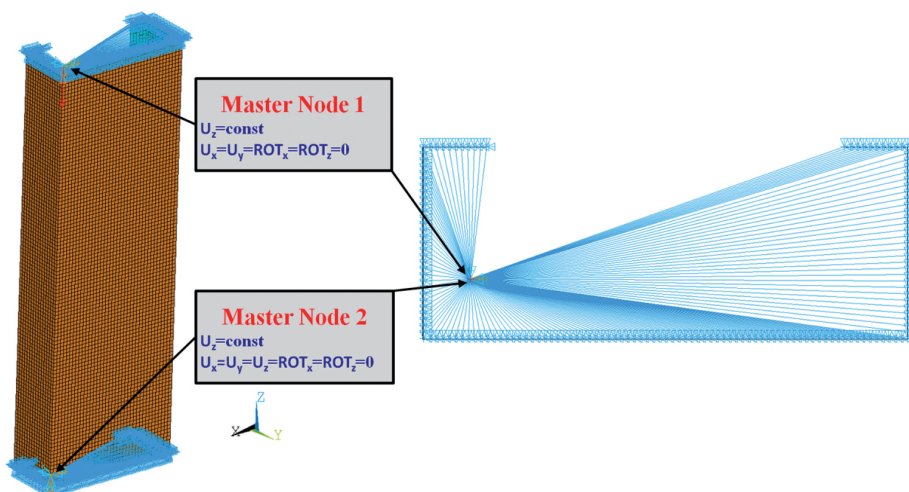


Fig. 3

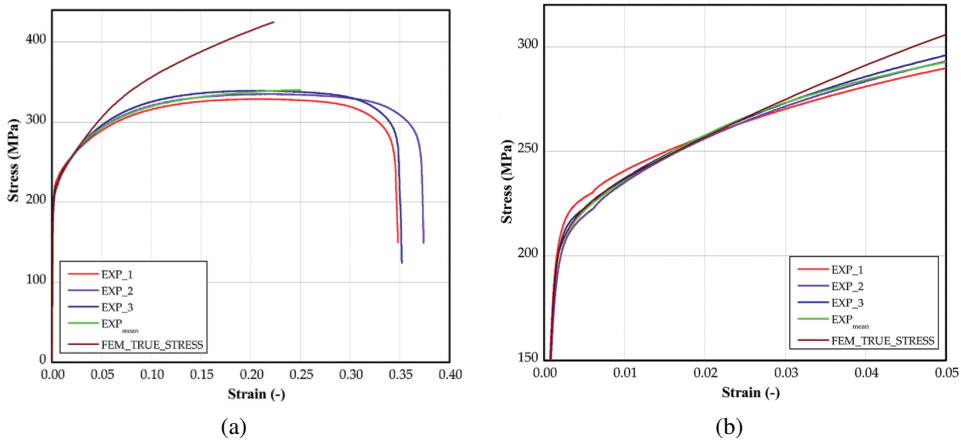


Fig. 4

3.2. Finite difference method (FDM)

Since a buckling mode of a mono-symmetric thin-walled cold-formed steel member with open cross-section may be global (flexural, flexural-torsional), local, distortional or interaction of different buckling modes can take place, one of the basic theories, which enables analysing the buckling, post-buckling, and ultimate strength of such members, is the Koiter asymptotic theory [8–10]. In order to derive pre- and post-buckling path of the member, the FDM solution was applied, based on Koiter's asymptotic method, that was adjusted to solve the stability problem of beam-columns subjected to compression and bending. This modification can be written as:

$$(3.1) \quad U = U_0 + \zeta U_1$$

where: U – field of displacements, U_1 – field of displacement describing buckling, post-buckling and part of prebuckling state, ζ – dimensionless parameter (equal to 1).

Equations (3.1) follows from perturbation theory for small values of parameter ζ . In analysis, this parameter is helpful to obtain linear equilibrium equations and it has only this usage. In the next step, differential equilibrium equations are solved using FDM. In this way, algebraic system of equations was obtained. Buckling state was solved using only linear part of differential nonlinear equilibrium equations. First, equilibrium equations were obtained from variation of potential energy of the beam-column and continuity equations were taken into consideration. Potential energy of beam-column is the sum of strain energy and work of load on total shortening. Strain energy for simple rectangular plate U can be expressed as product of stress tensor components and strain tensor components:

$$(3.2) \quad U = \iiint \{\sigma\}\{\varepsilon\}^T dV = \iint \{N_x, N_y, N_{xy}\}\{\varepsilon\}^T dA$$

where: V – volume of the plate, A – area of the plate and strain tensor component. They can be written as sum of linear and nonlinear parts of displacements and their derivatives according to formulae:

$$(3.3) \quad \varepsilon_x = u_{,x} + \frac{1}{2} \left(v_{,x}^2 + w_{,x}^2 \right)$$

$$(3.4) \quad \varepsilon_y = v_{,y} + \frac{1}{2} \left(w_{,y}^2 \right)$$

$$(3.5) \quad \gamma_{xy} = u_{,y} + v_{,x} + w_{,x}w_{,y}$$

In formula (3.2), derivative of v ($v_{,x}^2$) is used, because of in-plane bending of the plate (wall of beam-column). Taking constitutive equations and expressions (3.3), (3.4), (3.5) and (3.2), substituting into equation that expresses variation of potential energy, equilibrium equations can be written in form (3.6), (3.7) and (3.8):

$$(3.6) \quad Nx_{,x} + Nxy_{,y} = 0$$

$$(3.7) \quad Ny_{,y} + Nxy_{,x} = 0$$

$$(3.8) \quad Mx_{,xx} + 2Mxy_{,xy} + My_{,yy} + (Nx \cdot w_{,x})_{,x} + (Ny \cdot w_{,y})_{,y} + (Nxy \cdot w_{,y})_{,x} + (Nxy \cdot w_{,x})_{,y} = 0$$

Next, displacements u and internal forces N_x distributions of lipped-channel beam-column for $x = 0, L$ were assumed in form as follows:

$$(3.9) \quad u_1 = \frac{e1 + \frac{b3}{2} - b1 + y1}{e1 + \frac{b3}{2}} u_3(y3 = 0), \quad u_2 = u_4 = \text{const}$$

$$(3.10) \quad u_3 = \frac{e1 + \frac{b3}{2} - y3}{e1 + \frac{b3}{2}} u_3(y3 = 0)$$

$$(3.11) \quad u_5 = \frac{e1 - \frac{b3}{2} + y5}{e1 + \frac{b3}{2}} u_3(y3 = 0)$$

where: u_1 – u_5 – displacements of walls of analysed beam-column in x direction, y_1, y_3, y_5 – coordinates for walls of beam-columns in y direction, $u_3(y_3 = 0)$ – displacement of third wall of beam-column for $y_3 = 0$, e_1 – eccentricity, b_1, b_3 – width of first and third wall of beam-column,

$$(3.12) \quad Nx_{10}(y_1) = \frac{Nx_{40}(y_4) - Nx_{20}(y_2)}{b_3} (b_1 - y_1) + Nx_{20}(y_2)$$

$$(3.13) \quad Nx_{20}(y_2) = - \frac{(8b_1^3 - 12b_1^2b_3 + 6b_1b_3(b_3 + 2e_1) + b_3^2(6b_2(b_3 + 2e_1) + b_3(b_3 + 6e_1)))F}{16b_1^4 + 16b_1^3(b_2 - b_3) - 24b_1^2b_2b_3 + 8b_1b_3^2(3b_2 + b_3) + b_3^2(12b_2^2 + 8b_2b_3 + b_3^2)}$$

$$(3.14) \quad N_{x40}(y_4) = N_{x20}(y_2) * \varphi$$

$$(3.15) \quad N_{x30}(y_3) = N_{x20}(y_2) - y_3 * (N_{x20}(y_2) - N_{x40}(y_4))/b_3$$

$$(3.16) \quad N_{x50}(y_5) = \frac{N_{x40}(y_4) - N_{x20}(y_2)}{b_3} y_5 + N_{x40}(y_4)$$

where: $N_{x10}(y_1)$ – $N_{x50}(y_5)$ – internal forces on every edges of walls of beam-column, φ – coefficient obtained from conditions of equilibrium written for internal forces and moments, F – external force of compression for $x = L$:

$$(3.17) \quad u_1 = (b_1 - y_1) \frac{u_3(y_3 = b_3) - u_3(y_3 = 0)}{b_3} + u_3(y_3 = 0)$$

$$(3.18) \quad u_3 = (y_3) \frac{u_3(y_3 = b_3) - u_3(y_3 = 0)}{b_3} + u_3(y_3 = 0)$$

$$(3.19) \quad u_5 = (b_3 - y_5) \frac{u_3(y_3 = b_3) - u_3(y_3 = 0)}{b_3} + u_3(y_3 = 0)$$

After linearization of equilibrium equations and using finite difference schemes, algebraic linear system of equations were obtained and solved using Newton method and Mathematica 12.0 tool. Boundary conditions were assumed in this form (for $x = 0, L$):

$$(3.20) \quad v_i = 0, \quad w_i = 0$$

$$(3.21) \quad M_x = 0$$

$$(3.22) \quad \sum_{i=1}^N \int_0^{b_i} N_{x_i} dy_i = -F$$

$$(3.23) \quad \sum_{i=1}^N \int_0^{b_i} N_{x_i}(y_i) r_i(y_i) dy_i = F e_1$$

$$(3.24) \quad N_{y1} = 0, \quad M_{xy1} = 0, \quad M_{y1} = 0$$

$$(3.25) \quad N_{y5} = 0, \quad M_{xy5} = 0, \quad M_{y5} = 0$$

where: v, w – displacements in y and z directions (for i -th wall of beam-column), N_{y1}, N_{y5} – internal forces for wall no. 1 and 5, M_{xy1}, M_{xy5} – moments of torsion, M_{y1}, M_{y5} – bending moments, r_i – i -th distance from global axis of bending (symmetry axis of cross-section of beam-column) to i -th internal force N_{x_i} , N – number of walls of beam-column.

4. Experimental tests

The compression tests of columns eccentrically loaded with respect to major axis, were performed on Instron (Fig. 5a) testing machine. Also tensile tests of specimens taken from the profiles, carried out to determine mechanical properties of columns material were realized on the same machine. This machine allows performing tests for compression and

tension in the range of 0.2 kN to 200 kN. Tests of columns in eccentric compression were carried out in the special grip (Fig. 5a). In order to apply certain eccentric load to a column, special plates with grooves were employed (Fig. 5b). Columns were installed between two cradles and the cradles were bolted to the base plates enable angular motion. Their movable element is equipped with the exchangeable steel plate with grooves to place the short columns in it. Each groove corresponds to a certain eccentricity. The eccentricities of load in experiment were assumed to be between 0 and 60 mm. The greater value of e_x with respect to the dimensional restrictions of machine wasn't possible.

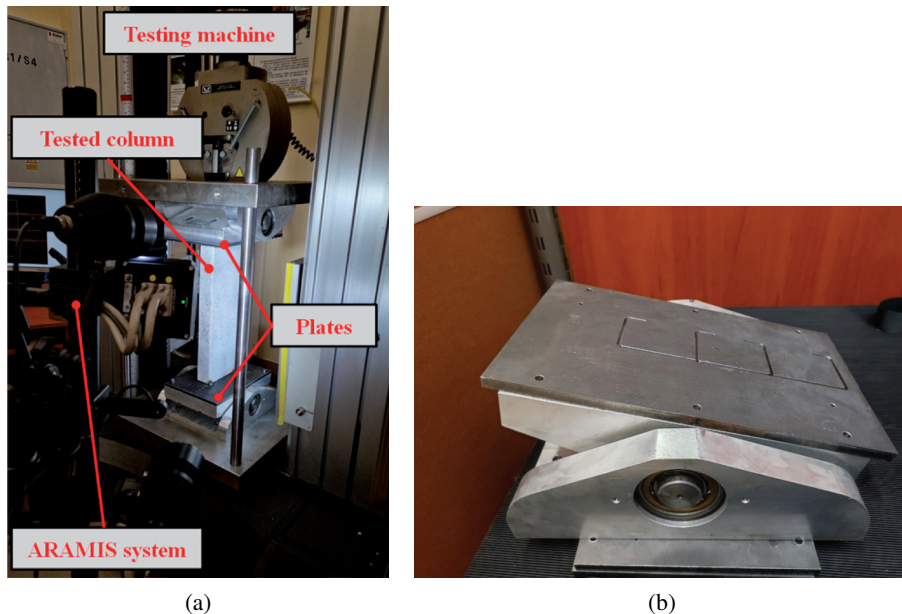


Fig. 5

5. Results of analysis

5.1. Equilibrium paths

This subsection shows the curves of compression load F vs. shortening S for several eccentricities e_x ranging from 0 mm to 120 mm. The critical (buckling) forces obtained by linear buckling analysis (LBA) and finite difference method (FDM), have been sorted out in Table 1. Fig. 6a presents the FE paths in full analysed range of shortening whereas in Fig. 6b the scope was limited to 2 mm to better see differences between curves. In general, for FE numerical approach with an increase of the eccentricity, the maximum load decreases and characteristics are similar (See Fig. 6).

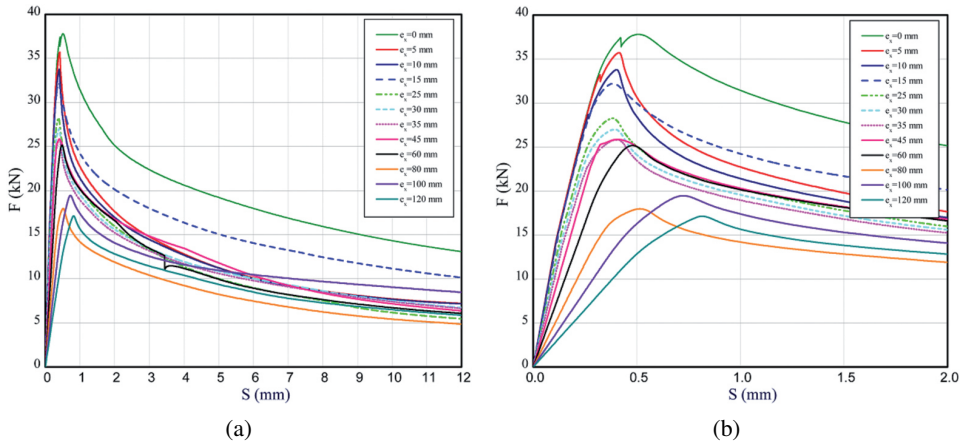


Fig. 6

Table 1. Buckling forces

Eccentricity (mm)	FDM (kN)	FEM (kN)
0	–	14.8
10	13.4	14.7
20	13.3	14.6
40	13.1	14.3
60	12.7	13.9
80	12.3	13.3
100	11.8	12.7
120	11.3	12.0

Taking a look at diagrams (Fig. 7 and Fig. 8) it is noticed that the curves for e_x between 30 mm and 60 mm some divergences occur (maximum loads registered for $e_x = 35$ mm, $e_x = 45$ mm and $e_x = 60$ mm were comparable). This could be caused by finding different equilibrium paths and different deformations of models during increasing load. Moreover, some paths ($e_x = 0$ mm, $e_x = 5$ mm, $e_x = 60$ mm) could suddenly change their trends due to appearance of local strains.

Fig. 7 and 8 present comparison of FE and FDM simulations, together with experimental results, for all eccentricities applied in the experimental tests. Additionally, in Fig. 7a an exemplary post-ultimate curve obtained on the basis of YLA method and developed using a preliminary theoretical plastic mechanism model shown, is presented. The agreement of FE and FDM results in the pre- and post-buckling range is very good. Experimental

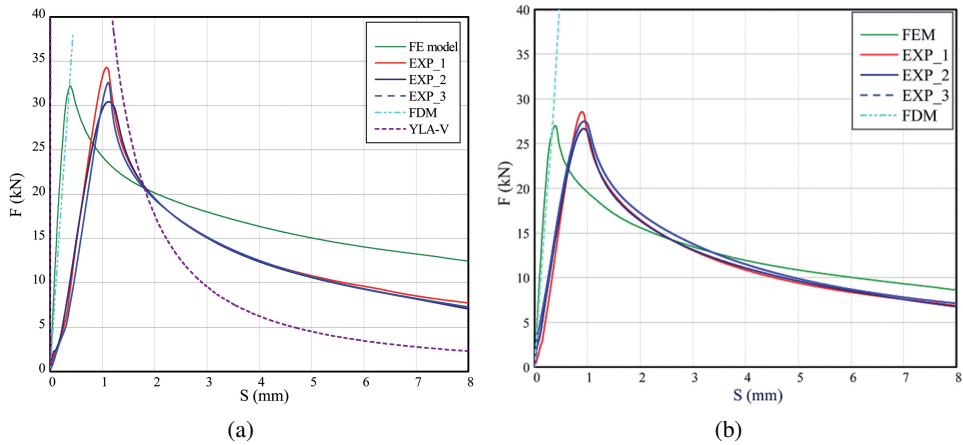


Fig. 7

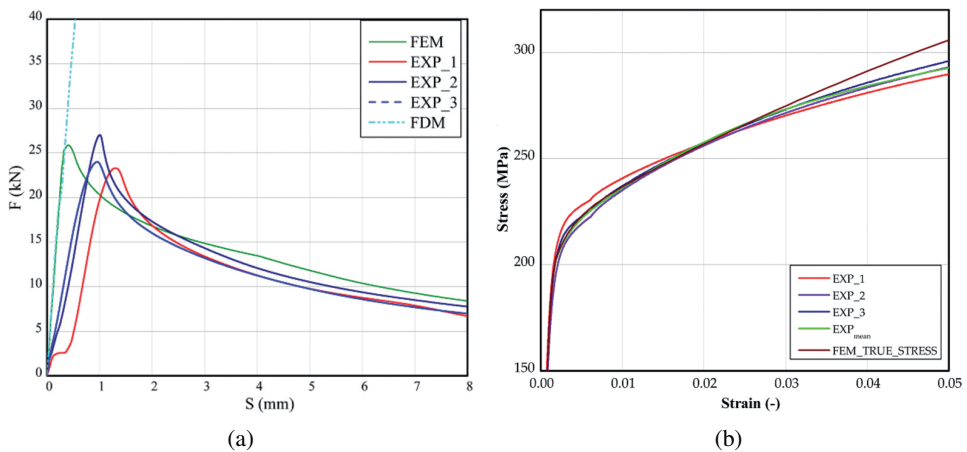


Fig. 8

paths indicate that the actual pre-ultimate stiffness of the columns is smaller. It is caused by initial geometrical imperfections of tested columns and minor differences between real and assumed boundary conditions. A character of the post-ultimate curve is similar to FE and experimental curves, but the mechanism model should be calibrated.

5.2. Deformation maps

The deformation maps obtained by DICAS and FE calculations are displayed in Table 2 and 3. Table 2 shows the maps for eccentricities 15 mm and 30 mm whereas Table 3 refers to cases with eccentricities 45 mm and 60 mm. The deformations maps were presented for

F_{max} obtained experimentally or numerically and two next lines in tables are displayed for higher loads (the same loads for both cases). Based on maps results, some correlations can be seen. At maximum loads of compression, maps are close (four or five waves appear, at most). In case of the experiments, plastic mechanisms were initiated and developed in the vicinity of the supports. In FE model, the points of the largest deformation were usually in the middle of profile (for $e_x = 30, 45, 60$ mm) or in two points (for $e_x = 15$ mm). Values of displacements appearing during experiment seem to be comparable. A qualitative agreement of experimental maps and FE simulations is satisfactory.

Table 2. Deformation maps for $e_x = 15$ mm and $e_x = 30$ mm

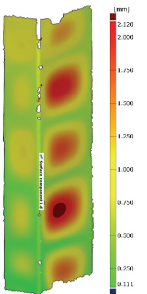
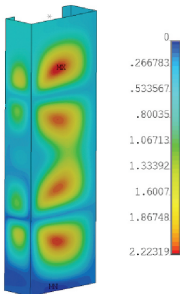
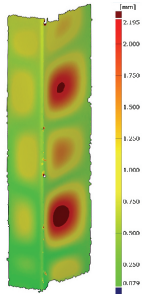
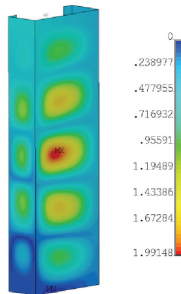
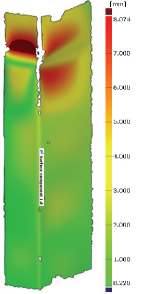
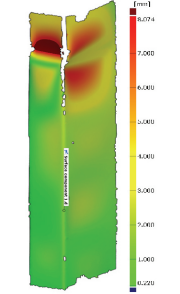
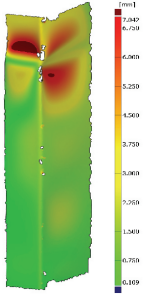
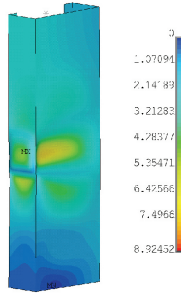
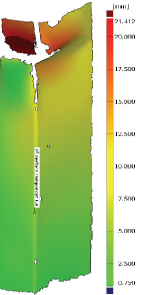
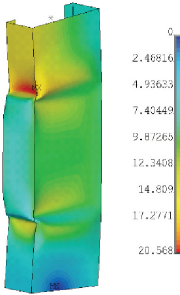
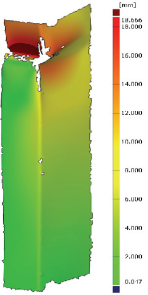
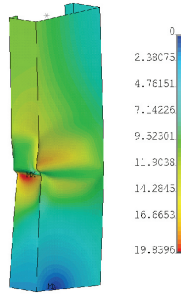
F (kN)	FEM	DICAS	F (kN)	FEM	DICAS
	$e_x = 15$ mm			$e_x = 30$ mm	
F_{max}			F_{max}		
15			13.8		
8.2			7		

Table 3. Deformation maps for $e_x = 45$ mm and $e_x = 60$ mm

F (kN)	FEM	DICAS	F (kN)	FEM	DICAS
	$e_x = 45$ mm			$e_x = 60$ mm	
F_{max}			F_{max}		
14.2			10.5		
8.1			5.8		

5.3. Load-carrying capacity

The diagrams of maximum loads versus eccentricity are presented in Fig. 9. The load-carrying capacities of analysed columns were showed based on results coming from FE calculations, experimental tests and analytical calculations based on Eurocodes 3 (EC3) [5, 6]. It is easily seen that numerical and experimental results are very close to each other. Numerical calculations for some eccentricities diverge from general trends. This divergence might be caused by numerical errors. The EC3 predictions underestimate the ultimate strength.

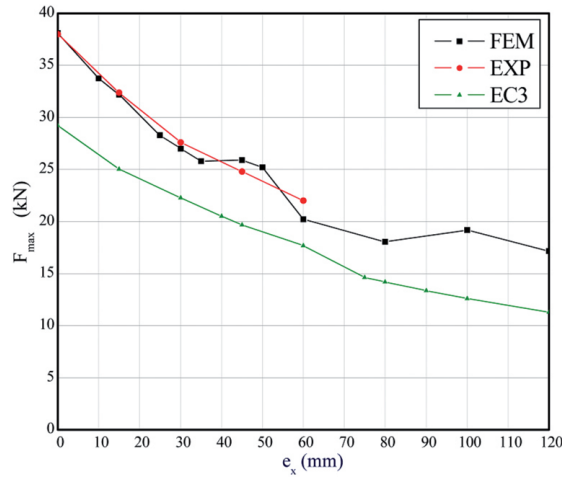


Fig. 9

6. Conclusions

The paper concerns the results of eccentric load of TWCFs based on two theoretical methods and experiment. Based on obtained results, some conclusions can be drawn:

1. The eccentric compression of columns about major axis causes a decrease in the maximum loads. It was observed that at the eccentricity of 120 mm load-carrying capacity dropped almost 2.5 times. Moreover, with regard to additional bending moment, deformation modes of profiles can be different.
2. Finite difference method (FDM) as an alternative approach used in present paper is in a good agreement with FE results. Critical loads of both methods differ slightly from each other but FDM usually gives smaller values (about 5–10%, at most).
3. Very preliminary results of YLA method used to determine post-ultimate curves are in a relatively good qualitative agreement with FE simulations and experiment. However, plastic mechanisms models should be very carefully calibrated using both DICAS deformation fields and 3D scanning procedures of failed specimens, which is planned in further research.
4. Thus, FDM approach together with YLA method can be applied in further development of relatively simple algorithms leading to the upper-bound estimation of the load-carrying capacity of columns subjected to eccentric compression. This approach should provide a more realistic prediction of the load-capacity than the effective width method.
5. Maximum loads estimated on the basis of EC3 for analysed columns gave lower values in a contrary to maximum loads achieved in experiments and in FE model (about 10–20%).

Acknowledgements

This work was supported by a grant 2019/35/B/ST8/02823 – Implementation of yield line theory to the load-capacity estimation of thin-walled members under combined load, of the National Science Centre of the Polish Ministry of Science and Higher Education.

References

- [1] Ansys, *User's Guide*, 18.2. Houston, TX, USA, 2018.
- [2] L. Borkowski, et al., "Ultimate and post-ultimate behaviour of thin-walled cold-formed steel open-section members under eccentric compression. Part II: Experimental study", *Thin-Walled Structures*, vol. 171, art. no. 108802, 2022, doi: [10.1016/j.tws.2021.108802](https://doi.org/10.1016/j.tws.2021.108802).
- [3] C. Buchanan, et al., "Cold-formed stainless steel CHS beam-columns – Testing, simulation and design", *Engineering Structures*, vol. 213, art. no. 110270, 2020, doi: [10.1016/j.engstruct.2020.110270](https://doi.org/10.1016/j.engstruct.2020.110270).
- [4] M. Chen and B. Young, "Numerical analysis and design of cold-formed steel elliptical hollow sections under combined compression and bending", *Engineering Structures*, vol. 241, art. no. 112417, 2021, doi: [10.1016/j.engstruct.2021.112417](https://doi.org/10.1016/j.engstruct.2021.112417).
- [5] EN 1993-1-1 Eurocode 3: Design of steel structures – Part 1-1: General rules and rules for buildings (including EN 1993-1-1:2005/AC, 2009). Brussels, Belgium: CEN, 2005.
- [6] EN 1993-1-3 Eurocode 3: Design of Steel Structures, Part 1.3: General Rules, Supplementary Rules for Cold-formed Thin Gauge Members and Sheeting. Brussels, Belgium: CEN, 2006.
- [7] B. Huang and W.F. Zhang, "Overall buckling performance of high strength steel welded I-sections under combined axial compression and bending", *Archives of Civil Engineering*, vol. 68, no. 3, pp. 369–384, 2022, doi: [10.24425/ace.2022.141891](https://doi.org/10.24425/ace.2022.141891).
- [8] W.T. Koiter, *General theory of mode interaction in stiffened plate and shell structures*, WTHD Report 590. Delft, 1976.
- [9] Z. Kołakowski and K. Kowal-Michalska, Eds., *Selected problems of instabilities in composite structures, A series of monographs*. Lodz: Technical University of Lodz Press, 1999.
- [10] Z. Kolakowski, "A semi-analytical method for the analysis of the interactive buckling of thin-walled elastic structures in the second order approximation", *International Journal of Solids and Structures*, vol. 33, no. 25, pp. 3779–3090, 1996, doi: [10.1016/0020-7683\(95\)00211-1](https://doi.org/10.1016/0020-7683(95)00211-1).
- [11] M. Kotełko, et al., "Ultimate and post-ultimate behaviour of thin-walled cold-formed steel open-section members under eccentric compression. Part I: Collapse mechanisms database (theoretical study)", *Thin-Walled Structures*, vol. 169, art. no. 108366, 2021, doi: [10.1016/j.tws.2021.108366](https://doi.org/10.1016/j.tws.2021.108366).
- [12] Q.Y. Li and B. Young, "Tests of cold-formed steel built-up open section members under eccentric compressive load", *Journal of Constructional Steel Research*, vol. 184, art. no. 106775, 2021, doi: [10.1016/j.jcsr.2021.106775](https://doi.org/10.1016/j.jcsr.2021.106775).
- [13] Y. Liang, et al., "Stainless steel channel sections under combined compression and minor axis bending-Part 1: Experimental study and numerical modeling", *Journal of Constructional Steel Research*, vol. 152, pp. 154–161, 2019, doi: [10.1016/j.jcsr.2018.03.027](https://doi.org/10.1016/j.jcsr.2018.03.027).
- [14] Y. Liang, et al., "Stainless steel channel sections under combined compression and minor axis bending-Part 2: Parametric studies and design", *Journal of Constructional Steel Research*, vol. 152, pp. 162–172, 2019, doi: [10.1016/j.jcsr.2018.03.028](https://doi.org/10.1016/j.jcsr.2018.03.028).
- [15] Y. Liang, et al., "Experimental and numerical studies of laser-welded stainless steel channel sections under combined compression and major axis bending moment", *Thin-Walled Structures*, vol. 157, art. no. 107035, 2020, doi: [10.1016/j.tws.2020.107035](https://doi.org/10.1016/j.tws.2020.107035).
- [16] X. Meng and L. Gardner, "Testing, modelling and design of normal and high strength steel tubular beam-columns", *Journal of Constructional Steel Research*, vol. 183, art. no. 106735, 2021, doi: [10.1016/j.jcsr.2021.106735](https://doi.org/10.1016/j.jcsr.2021.106735).

- [17] T. H. Miller and T. Pekoz, "Load-eccentricity effects on cold-formed steel lipped-channel columns", *Journal of Structural Engineering*, vol. 120, no. 3, pp. 805–823, 1994, doi: [10.1061/\(ASCE\)0733-9445\(1994\)120:3\(805\)](https://doi.org/10.1061/(ASCE)0733-9445(1994)120:3(805)).
- [18] G.P. Mulligan and T. Peköz, "Locally buckled thin-walled columns", *Journal of Structural Engineering*, vol. 110, no. 11, pp. 2635–2654, 1984, doi: [10.1061/\(ASCE\)0733-9445\(1984\)110:11\(2635\)](https://doi.org/10.1061/(ASCE)0733-9445(1984)110:11(2635)).
- [19] J. Rhodes and J.M. Harvey, "Interaction behaviour of plain channel columns under concentric or eccentric loading", in *Proc. 2nd Int. Colloquium on the Stability of Steel Structures*. Liege (Belgium): ECCS, 1977, pp. 439–444.
- [20] V. Ungureanu, et al., "Buckling strength and post-ultimate behaviour of lipped channel section short columns under eccentric compression", *Thin-Walled Structures*, vol. 181, art. no. 110085, 2022, doi: [10.1016/j.tws.2022.110085](https://doi.org/10.1016/j.tws.2022.110085).
- [21] O. Zhao, L. Gardner, and B. Young, "Structural performance of stainless steel circular hollow sections under combined axial load and bending – Part 1: Experiments and numerical modeling", *Thin-Walled Structures*, vol. 101, pp. 231–239, 2016, doi: [10.1016/j.tws.2015.12.003](https://doi.org/10.1016/j.tws.2015.12.003).
- [22] Y. Zhao, X. Zhai, and L. Sun, "Test and design method for the buckling behaviors of 6082-T6 aluminum alloy columns with box-type and L-type sections under eccentric compression", *Thin-Walled Structures*, vol. 100, pp. 62–80, 2016, doi: [10.1016/j.tws.2015.12.010](https://doi.org/10.1016/j.tws.2015.12.010).
- [23] L. Zhang, et al., "Experimental and numerical investigations of press-braked stainless steel channel section beam-columns", *Thin-Walled Structures*, vol. 161, art. no. 107344, 2021, doi: [10.1016/j.tws.2020.107344](https://doi.org/10.1016/j.tws.2020.107344).
- [24] L. Zhang, et al., "Press-braked stainless steel channel sections under major axis combined loading: tests, simulations and design", *Journal of Constructional Steel Research*, vol. 187, art. no. 106932, 2021, doi: [10.1016/j.jcsr.2021.106932](https://doi.org/10.1016/j.jcsr.2021.106932).

Analiza nośności mimośrodowo obciążonego stalowego słupa o przekroju ceowym

Słowa kluczowe: konstrukcje cienkościennie, nośność, obciążenie mimośrodowe, profil ceowy, teoria Koitera

Streszczenie:

Praca dotyczy analiz numerycznych, numeryczno-analitycznych i eksperymentalnych wpływu obciążeń mimośrodowych względem osi centralnej I_{\max} na pokrytyczne zachowanie i nośność cienkościennych zimno formowanych stalowych słupów o przekroju otwartym z żebrami końcowymi w pasach. Problem został rozwiązany stosując metodę elementów skończonych (program Ansys) z uwzględnieniem pełnych charakterystyk materiałowych w układzie logarytmicznym oraz nieliniowości geometrycznych. Rozwiązanie analityczno-numeryczne zostało oparte o teorię Koitera z zastosowaniem metody różnic skończonych. Wybrane wyniki symulacji zostały porównane z wynikami empirycznymi. Deformacje słupów podczas wykonywania badań doświadczalnych były rejestrowane optyczną metodą cyfrowej korelacji obrazów za pomocą systemu Aramis w celu określenia map deformacji i wielkości przemieszczeń punktów dla określonego obciążenia. Wyniki analizy pokazały, iż spadek w maksymalnych siłach w zależności od przesunięcia siły ściskającej względem osi centralnej słupa, może być nawet trzykrotny w odniesieniu do nośności ceowników ściskanych osiowo.

Received: 2023-04-18, Revised: 2023-05-16